PHYSICAL REVIEW E VOLUME 61, NUMBER 1 JANUARY 2000

Velocity and shape selection of dendritic crystals in a forced flow

X. Tong,[1] C. Beckermann,[1,*] and A. Karma[2]
[1]*Department of Mechanical Engineering, University of Iowa, Iowa City, Iowa 52242*
[2]*Department of Physics and Center for Interdisciplinary Research on Complex Systems, Northeastern University, Boston, Massachusetts 02115*

(Received 7 October 1999)

The phase-field method is used to simulate the two-dimensional growth of a dendritic crystal in a forced flow. The selection of the velocity and shape of the dendrite tip is investigated as a function of flow rate, growth direction relative to the flow, as well as anisotropy strength, and the results for the upstream growing tips are compared to existing theoretical predictions.

PACS number(s): 68.70.+w, 81.30.Fb

Dendritic growth is a well-known pattern formation problem of both fundamental and practical interest. By now, the subtle role of crystalline anisotropy in the selection of the dendrite tip size and velocity has been successfully explained by microscopic solvability theory [1]. Moreover, this theory has been recently validated by phase-field simulations in both two [2,3] and three dimensions [4] that focused on a purely diffusive regime. On earth, however, dendritic growth is almost unavoidably influenced by natural convection in the melt at low supercoolings [5], and the effect of fluid flow on the tip selection has remained somewhat unclear. On the theoretical side, models have been developed to predict how heat transport away from the tip is modified by flow in various situations [6–11]. In addition, Ben Amar and Pomeau [12] have proposed scaling laws to characterize the tip operating state in different regimes, and Bouissou and Pelcé [11] have extended the linearized solvability theory, which assumes a parabolic tip shape, to make quantitative predictions of velocity selection for the case of a uniform axial flow in two dimensions. On the experimental side, quantitative studies of flow effects on the tip selection have produced different results [13–16], such that there is still a clear lack of consensus.

In this Rapid Communication, we use a recently developed phase-field approach [17] to simulate directly the fundamental equations of solidification with flow. This allows us to investigate rigorously the effect of flow on the tip operating state for different anisotropy strengths and flow orientations relative to the growth direction, and thus to critically test quantitatively existing transport and solvability theories. Our approach is based on a methodology developed by Beckermann *et al.* [17] that incorporates melt convection phenomenologically in the phase-field model. In particular, the usual no-slip condition at a sharp solid-liquid interface is enforced in this approach through a varying interfacial stress term in the diffuse interface region. In addition, the results of the asymptotic analysis of Karma and Rappel [2,4] for the purely diffusive phase-field model, which extend to the convective case [17], are exploited to render our computations more efficient and to investigate the limit of vanishing interface kinetics (i.e., local equilibrium at the solid-liquid interface).

Let us first summarize the basic equations of our model. We use the anisotropic form of the phase-field equation (see Ref. [4] and earlier references therein) given by

$$\begin{aligned}\tau(\vec{n})\partial_t\psi &= \nabla\cdot[W^2(\vec{n})\nabla\psi] - \partial_\psi F(\psi,\lambda u)\\ &\quad + \partial_x[|\nabla\psi|^2 W(\vec{n})\partial_{\psi_x}W(\vec{n})]\\ &\quad + \partial_y[|\nabla\psi|^2 W(\vec{n})\partial_{\psi_y}W(\vec{n})],\end{aligned} \tag{1}$$

where ψ denotes the phase-field that varies smoothly from 1 in the solid to -1 in the liquid across a diffuse interface region, and $u=(T-T_m)/(L/C_p)$ is the dimensionless temperature field, where T_m is the melting point and L and C_p are the latent and specific heat, respectively. The function $F(\psi,\lambda u)=f(\psi)+\lambda u g(\psi)$ is a phenomenological free energy, where $f(\psi)=-\psi^2/2+\psi^4/4$ is a double-well function and $g(\psi)=\psi-2\psi^3/3+\psi^5/5$ is an odd function that preserves the minima of ψ at $+1$ and -1 when u is different from zero. The interface thickness is a function of the interface normal $\vec{n}$: $W(\vec{n})/W_0=A_s(\vec{n})$, with $A_s(\vec{n})=(1-3\varepsilon)+4\varepsilon(\psi_x^4+\psi_y^4)/|\nabla\psi|^4$, where ψ_x and ψ_y are first derivatives with respect to x and y and ε is the anisotropy strength of the surface energy. Using the results of Refs. [2,4], the limit of vanishing interface kinetics is achieved by choosing $\tau(\vec{n})=\tau_0[A_s(\vec{n})]^2$ with $\lambda=a_1W_0/d_0$ and $\tau_0=a_1a_2(W_0)^3/(d_0D)$, where d_0 is the capillary length and D is the thermal diffusivity, and where $a_1=0.8839$ and $a_2=0.6267$ for the functional forms of $f(\psi)$ and $g(\psi)$ given above. Therefore W_0 is the only free parameter that has to be properly chosen to obtain converged solutions. Next, the energy equation, including the advective flux, can be written as [17]

$$\partial_t u+(1-\phi)\vec{V}\cdot\nabla u = D\nabla^2 u+\partial_t\phi, \tag{2}$$

where we have defined the solid fraction $\phi=(1+\psi)/2\in[0,1]$ and $\vec{V}$ is the flow velocity. The conservation equations for mass and momentum take the following forms [17], respectively,

$$\nabla\cdot[(1-\phi)\vec{V}]=0, \tag{3}$$

*Author to whom correspondence should be addressed. FAX: (319) 335-5669. Electronic address: becker@engineering.uiowa.edu

$$\partial_t[(1-\phi)\vec{V}]+(1-\phi)\vec{V}\cdot\nabla\vec{V} = -(1-\phi)\nabla p/\rho+\nabla\cdot[\nu\nabla(1-\phi)\vec{V}]+\vec{M}_l^d, \quad (4)$$

where p, ρ [in Eq. (4) only], and ν are the pressure, density, and kinematic viscosity, respectively. The term $\vec{M}_l^d$ is the dissipative interfacial stress and is modeled as $\vec{M}_l^d = -2h\phi^2(1-\phi)\nu\vec{V}/W_0^2$, in which the constant h is found to be 2.757 by an asymptotic analysis of plane flow past the diffuse interface [17]. This term serves as a distributed momentum sink in the diffuse interface region that forces the liquid velocity to zero as $\phi\rightarrow 1$ and vanishes in the bulk liquid ($\phi=0$). An important property of this interfacial stress term is that the velocity profile near the diffuse interface smoothly approaches the profile for a sharp interface at $\phi=0.5$ (or $\psi=0$), regardless of the diffuse interface thickness. These and other details can be found in Ref. [17]. By rescaling length and time by W_0 and τ_0, respectively, we obtain a dimensionless version of the above equations. Then, all dimensional variables are cast into dimensionless forms as: $V\tau_0/W_0\rightarrow V$, $D\tau_0/(W_0)^2\rightarrow D$, $\nu\tau_0/(W_0)^2\rightarrow\nu$, $(p/\rho)(\tau_0/W_0)^2\rightarrow(p/\rho)$, while W_0 and τ_0 are set equal to unity.

Computations are performed in a square domain with a circular seed, initially at $u=0$, placed in the center. The melt, at $u_{\text{in}}=-\Delta$, enters from the top boundary with a uniform inlet velocity U, and leaves through the bottom boundary. Symmetry boundary conditions are applied at $x=0$ and the side boundary of the domain. The phase-field and energy equations are solved using an explicit Euler scheme [4], while the mass and momentum equations are integrated using an adapted version of the implicit multigrid code of Lilek, Muzaferija, and Peric [18]. The tip radii are evaluated from the computed phase-field contours using the method detailed in Ref. [4].

For a fixed supercooling of 0.55, Fig. 1 shows the computed evolution of dendritic crystals for three different anisotropy strengths without flow (top panels), and with flow (bottom panels). It can be seen that for all anisotropy strengths the shape of the crystals is significantly influenced by the flow. The upstream tip eventually reaches a steady state with a velocity that is much higher than the diffusive value, because the impinging flow reduces the thermal boundary layer thickness. The tip that grows in the horizontal direction normal to the flow also reaches an approximate steady state with a velocity that is about the same as the diffusion value. This is in qualitative agreement with the experiments of Bouissou, Perrin, and Tabeling [13] who found that σ^* does not depend on the transverse component of the flow. Note that in the presence of flow the horizontal tips grow slightly upwards due to the asymmetry of the heat fluxes on the sides of the horizontal arms. The evolution of the downstream arm in the wake of the crystal is retarded relative to the diffusion case, because of advection of heat from the upstream portion of the crystal. Moreover, the downstream tip does not reach a complete steady state due to the ever-increasing size of crystal.

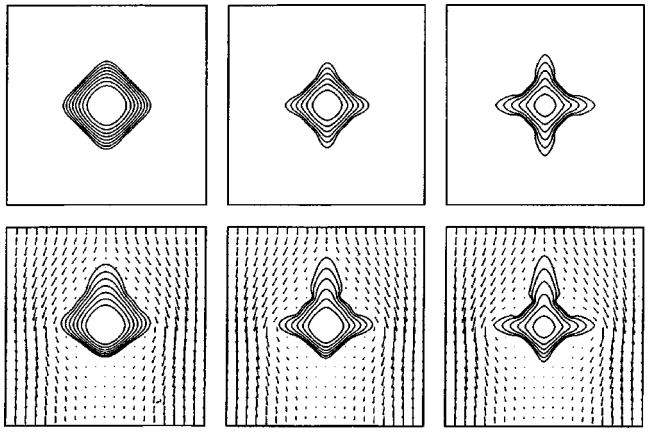

FIG. 1. Evolution of phase-field contours for $\Delta=0.55$ and $\varepsilon=0.01$, 0.03, and 0.05 (from left to right) without convection (top panels) and with convection (bottom panels) for a flow velocity of $Ud_0/D=0.07$ and a Prandtl number of Pr=23.1 (320×640 CVs with a uniform spacing of $\Delta x/W_0=0.4$).

The accuracy of the phase-field simulations with flow may be established by examining their convergence behavior in the thin-interface limit. Table I shows simulated steady-state upstream tip velocities and radii for decreasing values of the diffuse interface thickness (i.e., decreasing dimensionless diffusivity D in the limit of vanishing interface kinetics [2,4]) and different grid sizes. For each of the anisotropy strengths, converged results have been obtained.

Let us now compare our results to the predictions of the theory of Bouissou and Pelcé [11], which applies to the up-

TABLE I. Convergence study with flow: steady-state upstream tip velocity and radius for different grids and diffuse interface thicknesses ($\Delta=0.55$, Pr=23.1, and $\Delta x/W_0=0.4$). T_{CPU} denotes the CPU time in hours on a HP-C200 workstation; N_x and N_y are the number of grid points in the x and y directions, respectively.

ε	Ud_0/D	D	d_0/W_0	N_x	N_y	Vd_0/D	ρ/d_0	T_{CPU}
0.03	0.135	3	0.185	640	1280	0.0288	16.8	45
0.03	0.135	2	0.277	640	1280	0.0296	15.5	60
0.03	0.135	2	0.277	1024	2048	0.0286	14.9	120
0.03	0.135	1	0.554	1024	2048	0.0303	14.7	150
0.05	0.035	4	0.139	160	320	0.0265	8.10	3
0.05	0.035	4	0.139	288	576	0.0240	7.51	8
0.05	0.035	4	0.139	576	1152	0.0244	7.46	31
0.05	0.035	3	0.185	320	640	0.0248	7.48	17
0.05	0.035	2	0.277	512	1024	0.0247	7.61	70

stream tip in the present simulations. The main result of the transport of their theory is a supercooling-Péclet number relationship

$$\Delta = \mathrm{Pe}_c \exp(\mathrm{Pe}_c - \mathrm{Pe}_f) \int_1^\infty \left\{ -\mathrm{Pe}_c \eta + \mathrm{Pe}_f \times \left[2 + \int_1^\eta g(\zeta)/\sqrt{\zeta} d\zeta - \eta \right] \right\} / \sqrt{\eta} d\eta, \quad (5)$$

derived by assuming an isothermal parabolic tip growing in a low Reynolds number Oseen type flow in two dimensions. In Eq. (5), $\mathrm{Pe}_c \equiv V\rho/(2\mathrm{D})$ is the growth Péclet number, where the subscript c serves to distinguish it from the growth Péclet number obtained from simulations, $\mathrm{Pe}_f \equiv U\rho/(2\mathrm{D})$ is the flow Péclet number, and

$$g(\zeta) = \{ \sqrt{\zeta}\, \mathrm{erfc}(\sqrt{\mathrm{Re}\,\zeta/2}) + \sqrt{2/(\pi\,\mathrm{Re})} [\exp(-\mathrm{Re}/2) - \exp(-\mathrm{Re}\,\zeta/2)] \} / \mathrm{erfc}(\sqrt{\mathrm{Re}/2}) \quad (6)$$

is a function that depends on the Reynolds number, $\mathrm{Re} \equiv U\rho/\nu = 2\,\mathrm{Pe}_f/\mathrm{Pr}$. Equations (5) and (6) reduce to the well-known (two-dimensional) Ivantsov relation in the absence of flow ($\mathrm{Pe}_f = 0$). The main result of the linear solvability part of this theory is that the ratio $(\sigma^*)_0/\sigma^*$ of the selection parameters without and with flow (where σ^* is defined by $\rho^2 V \equiv 2d_0 D/\sigma^*$) is a function of a dimensionless parameter $\chi = a(\mathrm{Re}) d_0 U/(\beta^{3/4}\rho V)$, where $\beta = 15\varepsilon$ and $a(\mathrm{Re}) = \sqrt{2\,\mathrm{Re}/\pi}\exp(-\mathrm{Re}/2)/\mathrm{erfc}(\sqrt{\mathrm{Re}/2})$. This function is such that for $\chi > \chi_c$, where χ_c is a critical threshold value much larger than unity [11], this ratio has the asymptotic form $(\sigma^*)_0/\sigma^* \cong 1 + b\chi^{11/14}$ where b is a constant, whereas for χ much smaller than unity, as is the case in the present simulations, this ratio should be independent of flow velocity, i.e., $(\sigma^*)_0/\sigma^* \cong 1$. We verified and refined the latter prediction by evaluating numerically the complex solvability integral derived in Ref. [11] and found that $(\sigma^*)_0/\sigma^*$ increases about 1% over the range of $0 < \chi < 0.2$ that corresponds to our simulations.

The tip Péclet numbers (Pe) extracted from simulations are compared to the predicted values (Pe_c) from the Oseen-Ivantsov relation [Eqs. (5) and (6)] in Fig. 2 for $\Delta = 0.55$, $\mathrm{Pr} = 23.1$, flow Péclet numbers (Pe_f) ranging from 0 to 1 ($\mathrm{Re} < 0.1$), and three different anisotropy strengths ($\varepsilon = 0.01$, 0.03, and 0.05). While all the Péclet numbers increase with increasing flow velocity, the ones from simulations are significantly below the prediction of the Oseen-Ivantsov relation, with the gap between simulation and theory increasing with ε. This gap has been observed previously in a purely diffusive regime (e.g., see Ref. [4]) and is due to the fact that the interface shape deviates from a parabola close to the tip, with this deviation increasing steeply with anisotropy strength. By evaluating the local curvature of the simulated interfaces as a function of the distance, z, along the growth axis from the tip, we found that the deviation from a parabolic shape is limited to a distance no larger than about one tip radius. Further away from the tip, the interface shape is accurately fitted by a parabola, $z = x^2/2\rho_p$ (where x is the coordinate perpendicular to the growth axis), in agreement with the fact that a parabola is an exact solution of the steady-state growth equations for an isothermal interface within the Oseen approximation. Consequently, in order to meaningfully compare our results to the predictions of the Oseen-Ivantsov relation and the linearized solvability theory, which are both based on a parabolic shape, we must use ρ_p instead of the actual tip radius ρ when calculating the tip Péclet number and the selection parameter for our simulations. For this purpose, we extracted the ''parabolic'' tip radius, ρ_p, by measuring the slope of z versus x^2 in the region of the simulated interfaces behind the tip where this plot becomes a straight line. Note that ρ_p is likely to be the experimentally measured tip radius since a parabolic fit of the tip shape has been traditionally used to extract this parameter, even though it does not correspond to the actual tip

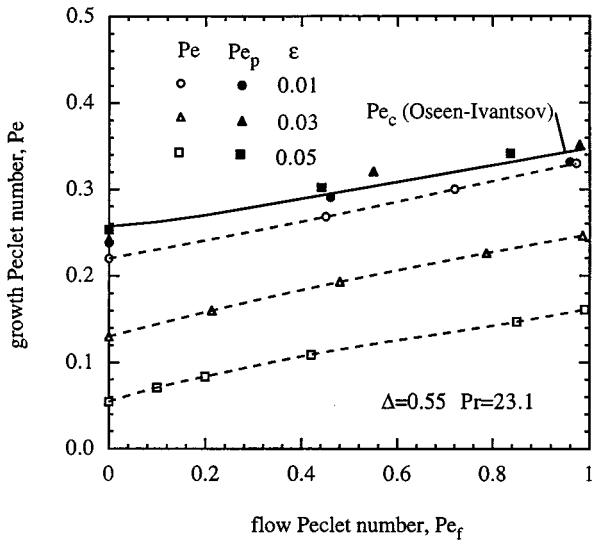

FIG. 2. Variation of the growth Péclet number with the flow Péclet number, and comparison with the two-dimensional Oseen-Ivantsov solution (solid line) [11]. Both the growth and flow Péclet numbers are evaluated using the actual tip radius ρ for the open symbols and dashed lines, and the radius ρ_p based on the parabolic fit for the solid symbols.

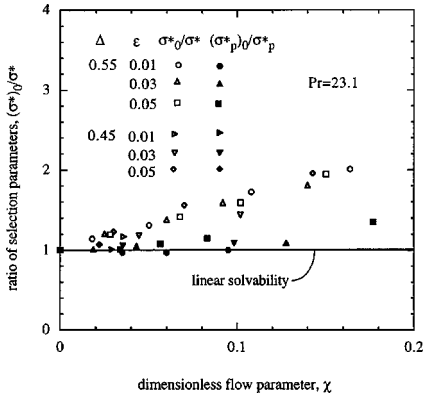

FIG. 3. Variation of the ratio of the selection parameters without and with flow as a function of the dimensionless flow parameter χ, and comparison with the linear solvability theory for a parabolic tip [11] (the theoretical lines for all three anisotropy strengths coincide). Both the ratio of the selection parameters and the flow parameter are evaluated using the actual tip radius ρ for the open symbols and the radius ρ_p based on the parabolic fit for the solid symbols.

radius. Using ρ_p and the tip velocity V from our simulations, we calculated a parabolic Péclet number, $\mathrm{Pe}_p = \rho_p V/2D$, and a selection parameter, $\sigma_p^* = 2\mathrm{D}d_0/(\rho_p^2 V)$. As opposed to Pe, Pe_p is in good agreement with Pe_c predicted from Eqs. (5) and (6) for all flow and anisotropy strengths, as shown in Fig. 2. In addition, Fig. 3 shows that the ratio $(\sigma_p^*)_0/\sigma_p^*$ of the parabolic selection parameters without and with flow is nearly independent of flow rate for all ε and Δ, in agreement with the prediction of the linearized solvability theory.

In contrast, Fig. 3 shows that the ratio $(\sigma^*)_0/\sigma^*$ of selection parameters based on the *actual* tip radius varies by about a factor of up to 2 over the range of flow velocities investigated, even though χ is small. This result shows that the flow distorts the interface shape (and thus influences ρ) within a distance of less than one ρ from the tip. The tip velocity, however, which is fixed by the transport relation and σ_p^* remains reasonably well predicted by the linearized solvability theory for not too large an anisotropy. This may seem surprising since this theory assumes a purely parabolic tip. We note, however, that this nontrivial feature of the linearized theory is already present without flow. In this case, the theory predicts reasonably well the tip velocity over a comparable range of anisotropy (in two and even three dimensions [19]) *despite* the presence of a tip distortion already induced by anisotropic surface tension alone. Our results therefore lead to the interesting conclusion that the shape deviation from a parabola on a short distance scale from the tip of a fraction of ρ, which is controlled by both anisotropy and flow, does not significantly influence the selection of ''measurable quantities'' such as the tip velocity and the tip shape on a larger scale of ten tip radii. Simulations at lower supercoolings, higher flow velocities, and in three dimensions remain an important challenge for the future.

We thank Professor Milovan Peric, Universität Hamburg, Germany, for providing the multigrid SIMPLE code. This work was supported by the National Science Foundation (NSF) under Grant No. CTS-9501389 and NASA under Contract No. NCC8-94. The research of A.K. was also supported by U.S. DOE Grant No. DE-FG02-92ER45471.

[1] J. S. Langer, in *Chance and Matter*, edited by J. Souletie, J. Vannenimus, and R. Stora (North-Holland, Amsterdam, 1987), p. 629; D. Kessler, J. Koplik, and H. Levine, Adv. Phys. **37**, 255 (1988); E. A. Brener and V. I. Mel'nikov, *ibid*. **40**, 53 (1991).

[2] A. Karma and W.-J. Rappel, Phys. Rev. E **53**, R3017 (1996).

[3] N. Provatas, N. Goldenfeld, and J. Dantzig, Phys. Rev. Lett. **80**, 3308 (1998).

[4] A. Karma and W.-J. Rappel, Phys. Rev. Lett. **77**, 4050 (1996); Phys. Rev. E **57**, 4323 (1998).

[5] M. E. Glicksman, S. R. Coriell, and G. B. McFadden, *Annual Review of Fluid Mechanics*, edited by M. Van Dyke (Academic Press, San Diego, CA, 1986), Vol. 18, p. 307; Y. W. Lee *et al.*, in *Annual Review of Heat Transfer*, edited by C. L. Tien (Begell House, New York, 1996), Vol. 7, p. 59.

[6] S. Dash and W. N. Gill, Int. J. Heat Mass Transf. **27**, 1345 (1984).

[7] D. A. Saville and P. J. Beaghton, Phys. Rev. A **37**, 3423 (1988).

[8] R. Ananth and W. N. Gill, J. Cryst. Growth **91**, 587 (1988).

[9] J.-J. Xu, J. Fluid Mech. **263**, 227 (1994).

[10] R. J. Sekerka, S. R. Coriell, and G. B. McFadden, J. Cryst. Growth **154**, 370 (1995).

[11] Ph. Bouissou and P. Pelcé, Phys. Rev. A **40**, 6673 (1989).

[12] M. Ben Amar and Y. Pomeau, Phys. Chem. Hydrodyn. **11**, 617 (1989).

[13] Ph. Bouissou, B. Perrin, and P. Tabeling, Phys. Rev. A **40**, 509 (1989).

[14] V. Emsellem and P. Tabeling, J. Cryst. Growth **156**, 285 (1995).

[15] Y. W. Lee, R. Ananth, and W. N. Gill, J. Cryst. Growth **132**, 226 (1993).

[16] R. Ananth and W. N. Gill, J. Cryst. Growth **179**, 263 (1997).

[17] C. Beckermann *et al.*, J. Comp. Phys. **154**, 468 (1999).

[18] Z. Lilek, S. Muzaferija, and M. Peric, Numer. Heat Transfer, Part B **31**, 23 (1997).

[19] A. Karma, Y. H. Lee, and M. Plapp, e-print cond-mat/9909021.